Transient Directed Motions of $GABA_A$ Receptors in Growth Cones Detected by a Speed Correlation Index

Cédric Bouzigues and Maxime Dahan
Laboratoire Kastler Brossel, Ecole normale supérieure, Centre National de la Recherche Scientifique UMR 8552 and Université Pierre et Marie Curie, Paris, France

ABSTRACT Single-molecule tracking of membrane proteins has become an important tool for investigating dynamic processes in live cells, such as cell signaling, membrane compartmentation or trafficking. The extraction of relevant parameters, such as interaction times between molecular partners or confinement-zone sizes, from the trajectories of single molecules requires appropriate statistical methods. Here we report a new tool, the speed correlation index, designed to detect transient periods of directed motion within trajectories of diffusing molecules. The ability to detect such events in a wide range of biologically relevant parameter values (speed, diffusion coefficient, and durations of the directed period) was first established on simulated data. The method was next applied to analyze the trajectories of quantum-dot-labeled $GABA_A$ receptors in nerve growth cones. The use of the speed correlation index revealed that the receptors had a "conveyor belt" type of motion due to temporary interactions ($\sim$4.0 s) between the receptors and the microtubules, leading to an average directed motion (velocity $\sim 0.3\ \mu m\ s^{-1}$) in the growth-cone membrane. Our observations point to the possibility of a cytoskeleton-dependent redistribution of the sensing molecules in the membrane, which could play a role in the modulation of the cell response to external signals.

INTRODUCTION

Over the past decade, single-molecule imaging has become an important tool for investigating the dynamics of cellular processes in live cells. The tracking of single membrane proteins has enabled the direct observation of important phenomena such as the compartmentation of the plasma membrane in microdomains (1–4), cell signaling in chemotaxis (5), or the trafficking of neurotransmitter receptors in the postsynaptic membrane (6–8). Imaging the motion of an individual protein is dependent on its biochemical labeling with an optically detectable probe used to locate the protein with a spatial accuracy of $\sim$10–40 nm. Probes as diverse as latex beads (8), gold nanoparticles (1,2,4), organic fluorophores (5), fluorescent proteins (3), or semiconductor quantum dots (QDs) (6,9) have been successfully employed to detect individual molecules in live cells.

In tracking experiments, the raw data are trajectories of individual biomolecules in the cell membrane. A crucial issue is how to extract physical information from these trajectories and to infer the molecular interactions that govern the motion. In most studies, one relies on a global analysis of the trajectory with the mean-square displacement (MSD) function, from which, for instance, the diffusion coefficient or the velocity can be determined (10,11). However, the computation of the MSD results from the averaging of displacements along the whole trajectory. This analysis is thus only suitable for biomolecules for which the motion features (diffusion coefficient, velocity, etc.) do not change during the course of the trajectory. As a consequence, local or transient changes in the lateral dynamics cannot be detected by means of the MSD. Their identification requires appropriate statistical tools, as shown for the detection of temporary confinements of diffusing particles (12,13)

In this article, we report a new statistical tool to detect transient directed motions based on the analysis of the temporal correlations of the speed of an individual molecule. It relies on the fact that these correlations are nonzero for a directed movement, but vanish for a Brownian motion. The method, termed the speed correlation index (SCI), was first validated on simulated trajectories. Next, it was applied to study the motion of $GABA_A$ receptors ($GABA_A$Rs) in the membrane of nerve growth cones (GCs). Gamma amino butyric acid (GABA), a common inhibitory neurotransmitter in the mature nervous system, is also known to serve as a chemoattractant in the developing system (14,15). Understanding the factors that regulate the membrane dynamics of the $GABA_A$Rs is therefore important for elucidating the spatiotemporal organization of the signal transduction cascade (16). By means of the SCI, we identified and characterized a dynamic equilibrium in which $GABA_A$Rs alternated between free Brownian diffusion and microtubule-dependent directed movement. In the literature, this type of lateral dynamics, termed a conveyor-belt motion (11,17), has previously been discussed in theoretical models but has seldom been identified in experiments. The coupling of signaling membrane molecules with the cytoskeleton raises the question of how the spatiotemporal organization of the chemoreceptors might participate to gradient sensing by nerve GCs.

Submitted August 1, 2006, and accepted for publication October 3, 2006.

Address reprint requests to Maxime Dahan, E-mail: maxime.dahan@lkb.ens.fr.

0006-3495/07/01/654/07 $2.00

doi: 10.1529/biophysj.106.094524

METHODS

Generation of synthetic trajectories

Synthetic trajectories were generated to test the SCI method. These trajectories were composed of 1024 points corresponding to the successive positions of a single molecule with a time increment $\tau = 75$ ms. The motion is a random walk except for a period during which there is an additional directed motion. The duration of this period is a random variable determined by an exponential distribution (a Poisson process) with a given characteristic time T. The displacement between two consecutive frames is $\xi(t)$, a two-dimensional Gaussian variable of variance $2D\tau$ in each direction (D is the diffusion coefficient, constant during the trajectory), during the phases of Brownian motion and the sum of $\xi(t)$ and of a constant displacement $v\tau$ in one direction (v is the speed of drift) during the phase of directed motion.

Principle of the SCI

The SCI is based on the fact that temporal correlations of the speed exist in directed motions, whereas they vanish on average for a purely Brownian motion. Thus, estimating the local correlations should provide an indicator of the nature of the motion. However, to analyze a single trajectory, it is necessary to perform averaging in an appropriate time window to achieve a local analysis while suppressing the noise inherent to trajectories with a Brownian component. One way to satisfy these two seemingly antagonistic requirements is presented below. The algorithm was inspired by the confinement index introduced to discriminate between free and confined diffusion. (12)

Let us consider a discrete trajectory containing N points corresponding to the consecutive positions of the particle at times $i = 1...N$. We define an averaging window of size L, and consecutive points inside the trajectory are pooled in segments of length L. It is possible to regroup the points of the trajectory into L different sets of segments (indexed by $k = 1...L$) by shifting the origin by 0,1,...$L - 1$ frames (Fig. 1). These families of segments are designated by $\{S_k(j)\}$, where j is the segment number in the set k. Frames at the beginning or at the end of the trajectory, such that $i < L$ or $N - i < 1$, are not part of a segment for certain values of k. (Fig. 1). We thus only consider in the final result of the computation the points i where $L < i < N - L$.

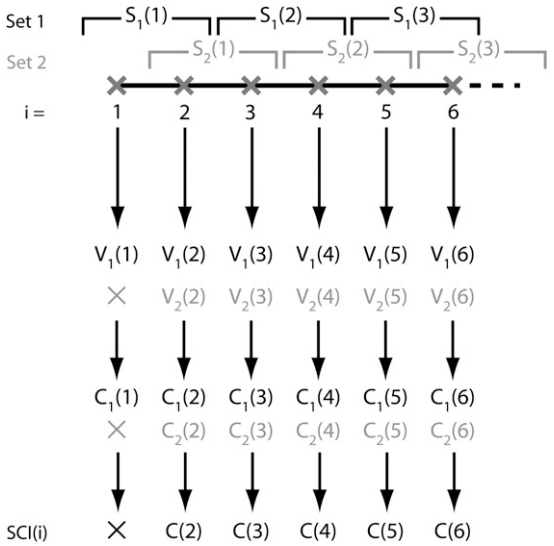

FIGURE 1 Principle of the algorithm in the case $L = 2$. Two sets of segments are defined (S_1 and S_2), providing two sets of speeds and correlations, V_1 and V_2, and C_1 and C_2, respectively (C_2 is not defined for the frame $i = 1$). The averaging of correlations yields the value C of the speed correlation index.

For each different set k, we compute the average two-dimensional velocity $\mathbf{U}_k(j)$ over the full segment $S_k(j)$, and attribute it to every point i within the segment j. The velocity for the point i belonging to the segment j in frame k is thus $\mathbf{V}_k(i) = \mathbf{U}_k(j)$. By repeating this operation for each set k of segments, one gets the array $\{\mathbf{V}_k(i)\}_{k=1..L}$. The correlation for the point i in the set k, $C_k(i)$, is given by:

$$C_k(i) = \frac{\mathbf{U}_k(j) \times \mathbf{U}_k(j+1)}{\|\mathbf{U}_k(j)\| \times \|\mathbf{U}_k(j+1)\|},$$

(where $\mathbf{U}_k(j) \times \mathbf{U}_k(j+1)$ is a scalar product). For each position i, the value $C(i)$ of the SCI is then obtained by averaging $C_k(i)$ for all the different values of k (Fig. 1):

$$C(i) = \langle C_k(i) \rangle_{k=1...L}.$$

With this definition, $C(i) = 0$ on average for a Brownian motion. In the opposite case of a directed motion with constant speed orientation and no additional Brownian diffusion, $C(i) = 1$.

The algorithm presented above is not notably modified for trajectories with periods (such as blinking events) during which the particle is not detected. In that case, when frames are missing in a given segment j, the average velocity $\mathbf{U}_k(j)$ is computed between the two most distant frames for which the particle was detected. As a consequence, it is not possible to compute the SCI on a trajectory containing blinking events that are longer than the length L. At any rate, it is possible to divide the trajectory into different parts with no blinking events longer than L and to concatenate the different parts of the computed SCI.

Optimization of parameters

The choice of the size L of the averaging window is important to optimize the procedure. If L is too short, no directed motion can be extracted from the data due to the Brownian noise, and if L is too long, the SCI does not provide any local information. The greater the value of the speed v is, the shorter the chosen L can be. A minimal possible value for L is one where the displacement due to the drift is comparable to the diffusion during the time $L\tau$: $4DL\tau \approx v^2L^2\tau^2$, i.e., $L \approx 4D/v^2\tau$. When the diffusion coefficient and the speed are chosen as $D = 0.25\ \mu m^2\ s^{-1}$ and $v = 0.8\ \mu m\ s^{-1}$, a choice of L between 20 and 35 frames is suitable. In the following analysis, we used $L = 30$ frames.

On synthetic trajectories simulating a conveyor-belt motion (Fig. 2 *A*), one observes phases during which $C(i)$ is high, ~1 (Fig. 2 *B*), possibly corresponding to periods of directed motion. To quantitatively identify these phases, a proper thresholding procedure needs to be defined for the curves $C(i)$. In particular, it is necessary to discriminate between ''true'' directed motions and stochastic fluctuations due to Brownian motion. We have thus developed an approach to define a threshold of confidence such that phases for which C is above the threshold have <5% probability of being due to Brownian fluctuations. For that purpose, we generated 100 purely Brownian trajectories for different values of the threshold H_c ($H_c = 0.90$, 0.85, 0.80, 0.75, 0.65, and 0.6). By computing the SCI on these trajectories, we determined the frequency with which C remains $>H_c$ during a certain number of consecutive frames. This provides an estimate of the probability $p(H_c,T)$ of observing a SCI $>H_c$ for a time longer than T only because of stochastic fluctuations. We then defined the critical duration T_c such that $p(H_c,T_c) = 0.05$ (Fig. 2 *C*). Only events for which C is higher than a given H_c during a period longer than T_c are considered significant and are due to directed motion. To measure the duration of phases of directed motion, we look at the lowest H_c for which we can detect a significant event of high SCI.

Experimental methods

Primary cultures of interneurons were obtained from the spinal cords of Sprague-Dawley rat embryos at E14 (Janvier, Le Genest St. Isle, France)

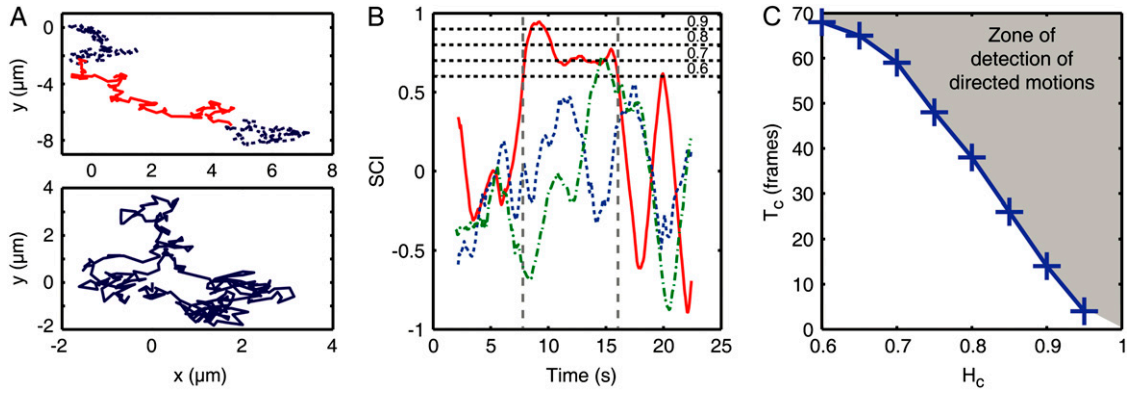

FIGURE 2 (*A*) Example of simulated trajectories with a period of directed motion (*upper*) with velocity $v = 0.8\ \mu m\ s^{-1}$ (*solid line*, between 8.7 s and 15.6 s) and purely Brownian (*lower*). (*B*) SCI for the directed trajectory (*solid line*) and two Brownian trajectories (*dash-dotted line*). The thresholding procedure enables the detection of the directed period (between 8.0 s and 15.9 s). Due to random fluctuations, high values of the SCI can be reached in Brownian trajectories for short durations. (*C*) Threshold determination. A part of the SCI curve above the height H for a continuous time T is indicative of a directed motion if the point of coordinates (H,T) is in the gray region on the graph.

(18). Spinal cords are dissociated in trypsin-EDTA 2.5% and by mechanical separation in 0.005 mg/ml DNase (Sigma-Aldrich, St. Louis, MO). Cells are plated on 60 μg/ml polyornithine-coated glass coverslips (Sigma-Aldrich) and incubated in glutamine (Invitrogen, Carlsbad, CA) and B27 (Invitrogen) supplemented with Neurobasal medium (Invitrogen) at 37°C under 5% CO_2. Cells are mounted before experiments in minimal essential medium (Sigma-Aldrich) supplemented with glutamine and B27, and kept in that medium for the duration of the experiments. γ2 subunits of $GABA_A$ receptors are sequentially labeled with guinea pig anti-γ2 antibodies (gift of J. M. Fritschy), Fab fragment of biotin-goat anti-guinea pig antibody (Rockland Immunochemicals, Gilbertsville, PA), and streptavidin-coated quantum dots (QDot, Hayward, CA). Receptors are imaged by epifluorescence (IX71 microscope with 60×, NA = 1.4 objective, Olympus, Tokyo, Japan). Single quantum dots were identified by their blinking. Image sequences were acquired at a rate of 13 Hz.

Custom-made software (Mathworks, Natick, MA) allowed us to reconstruct trajectories of single QDs in the sequence (19). The point spread function (PSF) of the optical system was measured by imaging single quantum dots spin-coated on a coverslip. The cross-correlation of each image in the sequence with a Gaussian approximation of the PSF is computed, and its local maxima above a user-defined threshold indicate the positions of the fluorescent nanoparticles. A Gaussian fit around detected maxima allows the detection of the spot positions with ~10 nm accuracy. The association of spots of different images within trajectories is based on a nearest-neighbor rule. For each spot detected in the k^{th} image of a sequence, we computed the probability of its belonging to a trajectory ending in one of the P precedent images of the sequence. P is a parameter accounting for the blinking of the QDs, which in practice is equal to 10 (meaning that P is inferior to the averaging window L). The computation is made by assuming that all the trajectories are Brownian with a diffusion coefficient estimated on the reconstructed part of the trajectories. After computation, each spot in the k^{th} image is then associated to the trajectory to which it is most likely to belong.

For each trajectory, we first computed the MSD versus time function between 0 and $T_{tot}/5$ where T_{tot} is the trajectory duration. The presence of a directed motion was determined using a criterion introduced by Kusumi et al. (20). In brief, the instantaneous diffusion coefficient D was measured by fitting the first five points of the MSD curve. For a trajectory where $MSD(T_{tot}/5) > 4D(T_{tot}/5)$, the MSD between 0 and T_{tot} was adjusted with a quadratic curve $4Dt + v^2t^2$. Based on the values of D, v, and T_{tot}, the statistical error was estimated at $t = T_{tot}/5$. A trajectory was considered directed when the MSD departed from the diffusive approximation $4Dt$ by >1 standard deviation. The SCI method was then applied to identify local periods of directed movements.

RESULTS

Synthetic data

We first generated 100 ''conveyor-belt'' trajectories with a Brownian component $D = 0.25\ \mu m^2\ s^{-1}$ and containing a single phase of directed movement with velocity $v = 0.8\ \mu m\ s^{-1}$. The duration of this phase was given by an exponential distribution with parameter $T = 4.1$ s. We computed the SCI for each trajectory and applied the detection method for the phases of directed motion. Using that set of parameters, 65% of all events were detected by the SCI analysis. Most of the lost events were those with a short duration. However, this does not have a substantial effect on the estimate of the drift time. The distribution of measured durations has a correct exponential shape with a mean value $T_m = 4.5$ s. (Fig. 3 *A*).

Next, we repeated the above analysis by varying the value of important parameters. The efficacy of detection is highly dependent on the relative values of the velocity v, the diffusion coefficient D, and the duration T of the directed motion. In our simulations, we used a fixed value of $D = 0.25\ \mu m^2\ s^{-1}$, typical for a protein freely diffusing in the plasma membrane (21). We generated trajectories with velocity v varying between 0.2 and 1.5 $\mu m\ s^{-1}$, consistent with the range of velocities observed in the motion of molecules or organelles in live cells. In addition, for each value of v, we varied the duration T from 2.25 to 8 s. Shorter events are not easily detectable due to the length of the averaging window.

For a given value of T, the detection of directed-motion periods was, as expected, more efficient for higher values of velocity, with a detection probability of between 25% and 80% in the range of parameters considered (Fig. 3 *B*). Similarly, for a given value of v, the detection rate increased with T (Fig. 3 *C*). This result is explained by the difficulty of detecting the shortest events of the distribution, which are more frequent for a smaller T. However, the measured time

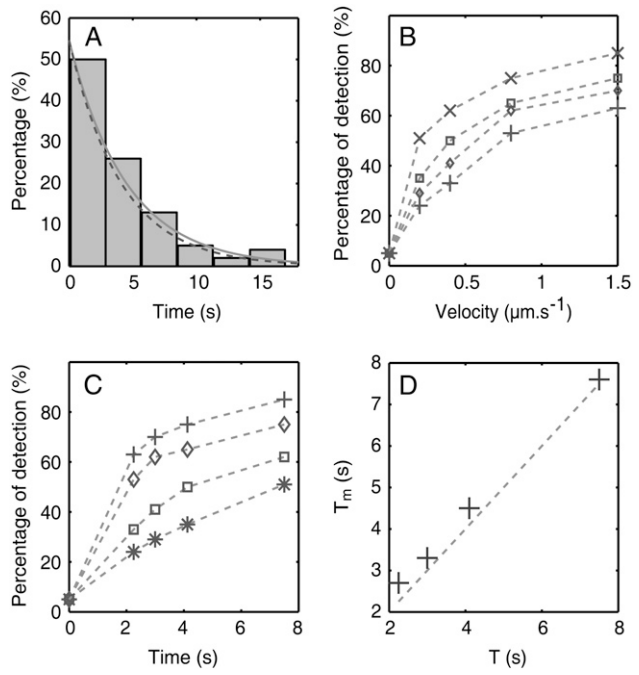

FIGURE 3 (*A*) Distribution of detected drift times in simulated trajectories (bins) and the resulting exponential fit with $T_m = 4.5$ s (*solid curve*), compared to the exponential distribution with $T = 4.1$ s (*dashed curve*) used as input in the simulation. (*B* and *C*) Percentage of detection as a function of (*B*) the velocity v for $T = 2.25$ s (+), 3 s (◇), 4.1 s (□) and 8 s (X), and (*C*) the average duration T for $v = 0.2$ μm s^{-1} (*), 0.4 μm s^{-1} (□), 0.8 μm s^{-1} (◇) and 1.5 μm s^{-1} (+). In all the trajectories, D was equal to 0.25 μm^2 s^{-1}. (*D*) Average duration T_m of the directed periods as a function of the duration T used in the simulation.

T_m remained close to the input parameter T of the simulation (Fig. 3 *D*), with the relative error decreasing from ~20% for $T = 2.25$ s to 1% for $T = 7.5$ s. This error is slightly biased, since the average duration T_m of the directed motions is overestimated by the SCI.

Altogether, the results indicate that, by means of the SCI, periods of directed movements can be identified and characterized over a wide range of speeds and durations. With our chosen sets of velocity and diffusion coefficient, the efficacy of the analysis method breaks down when the mean duration T is <1 s. The simulations presented here have been specifically designed to test the ability of the method to reveal exponential distribution of directed periods, but the SCI is in fact suitable for the detection of periods distributed according to other types of probability law, provided that their average duration is long enough.

Experimental data

The motions of single $GABA_A$Rs in GC membranes were recorded in the central region of the GC or in the lamellipodia. In the microtubule-rich central region, the MSD had a quadratic shape in 78% of individual trajectories (Fig. 4, *A–C*). The trajectories had no preferred orientation, indicating that they were not due to retrograde actin flow. By adjusting the MSD in each trajectory with a curve $4Dt + v^2t^2$, we determined the distributions of the velocity v and diffusion coefficient D. The average values (±SEM) were $v_{av} = 0.29 \pm 0.02$ μm s^{-1} and $D_{av} = 0.25 \pm 0.01$ μm^2 s^{-1} ($n = 92$), respectively (Fig. 4, *D* and *E*). In contrast, the receptors moving in the actin-rich lamellipodia had on average a purely Brownian motion ($D = 0.26 \pm 0.02$ μm^2 s^{-1}, $n = 38$). When the microtubules (MTs) were depolymerized by nocodazole (1 μM, 1 h), <5% ($n = 103$) of the MSD curves had a quadratic component, indicating that the directed motion had been almost entirely abolished (Fig. 4 *C*). After washing neurons extensively and letting them recover for 1 h in fresh medium to allow microtubule polymerization, 80% of $GABA_A$Rs had a directed motion (Fig. 4 *C*) with an average velocity $v = 0.28 \pm 0.03$ μm s^{-1} ($n = 35$) (Fig. 4 *F*), very similar to the velocity value before applying the drug. Altogether, these observations indicate that the directed motion of $GABA_A$Rs in the GC membrane was due to the microtubules.

The directed motion was next analyzed with the SCI (Fig. 5, *A* and *B*). In 64% of these trajectories, we detected the presence of temporary directed motion. To check the consistency of our analysis, we computed the MSD on parts of the trajectories identified as purely Brownian and found that the average MSD was linear (Fig. 5 *C*). The motion of the receptors is therefore not the result of a permanent drift combined with Brownian diffusion but consists of transient periods of directed motion, and can thus be designated as conveyor-belt movement (11,17). This reflects the existence of an equilibrium between two distinct ''dynamic states'' for the $GABA_A$Rs: a state in which they interact with microtubules and one in which they diffuse freely (Fig. 6).

When calculated for the directed periods only, the MSD varied quadratically with a velocity $v_{inst} = 0.75 \pm 0.04$ μm s^{-1} ($n = 59$) (Fig. 5, *D* and *E*). The diffusion coefficient $D = 0.26 \pm 0.02$ μm^2 s^{-1} ($n = 59$) was not significantly different from the value determined on the complete trajectories. The durations of the directed phases are exponentially distributed, with a mean value of 4.0 s (Fig. 5 *F*). This observation is indicative of a one-step process and suggests that $GABA_A$Rs unbind from microtubules at a rate $k_{off} = 0.25$ s^{-1}.

The nature of the microtubule-dependent motion of the receptors remains to be determined: are receptors actively moving along a microtubule (through interactions with a molecular motor) or are they carried during the microtubule polymerization? Although it was not possible to fully discriminate between the two models, several experimental facts led us to favor the latter hypothesis. First, the average elongation speed of microtubules in nerve GCs, previously determined by tracking GFP-tagged end-binding proteins, is equal to ~0.3 μm s^{-1} (22), close to the average velocity v_{av} obtained for the receptors' motion. Second, when the microtubules were frozen in their polymerized state by the action of taxol (1 h in 10 μg ml^{-1}), the MSD had a negative curvature. This could be interpreted as evidence for either

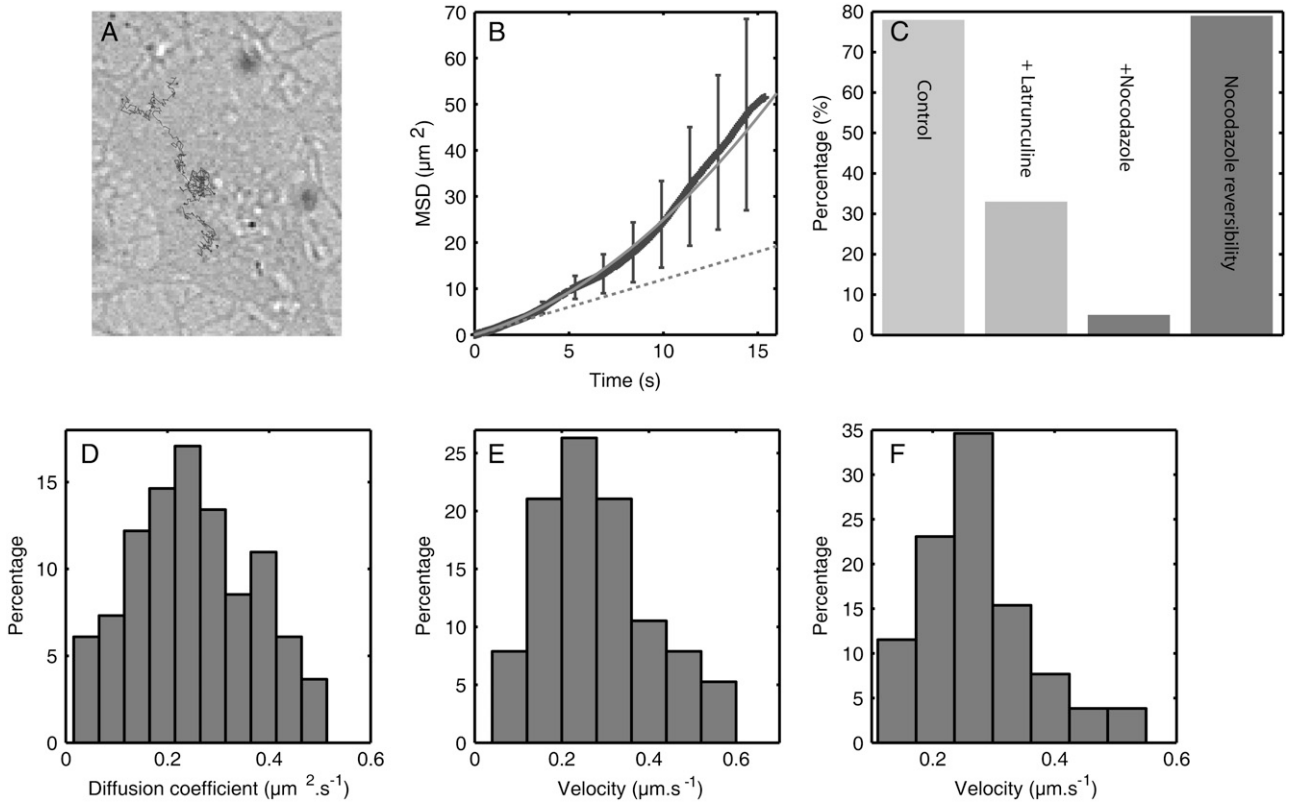

FIGURE 4 (*A*) Trajectory of a single $GABA_AR$ in the GC membrane. (*B*) MSD computed between 0 and $T_{tot}/5$ with a quadratic fit $4Dt + v^2t^2$ ($D = 0.30\ \mu m^2\ s^{-1}$, $v = 0.35\ \mu m\ s^{-1}$). (*C*) Proportion of directed trajectories in the control case and after drug treatment. (*D* and *E*) Distribution of diffusion coefficients and velocity of $GABA_AR$s in the control case. (*F*) Distribution of velocity after microtubule depolymerization by nocodazole and 2-h recovery in free medium.

anomalous diffusion $MSD(t) = 4Dt^a$ ($a \approx 0.9$) or a confined motion $MSD(t) = L^2(1 - e^{-4Dt/L^2})$ in a region of typical size $L = 2.6\ \mu m$. In either case, it excludes the possibility that receptors have a directed movement and underlines that the microtubule dynamics is the cause for the receptor transport (Fig. 6). In addition, the receptors appeared to be mostly confined to a region close to the limit between the central and peripheral regions of the GC, where the microtubule ends are located.

We also sought to evaluate the specific role of actin filaments. Depolymerization by a latrunculin A treatment (3 μM during 20 min) caused a reduction from 80% to 35% in the fraction of receptors having a directed motion. The average speed of these motions was $v_{lat} = 0.29 \pm 0.02\ \mu m\ s^{-1}$ ($n = 38$), comparable to the velocity in the control case. Since receptors in the lamellipodia do not exhibit directed motion, actin seems to be involved, but only indirectly, in the receptor locomotion. The decrease in the fraction of directed movement possibly results from the change in the microtubule dynamics induced by an alteration of the actin network (23–25).

DISCUSSION

The development of a new statistical tool, the speed correlation index, combined with single quantum-dot imaging has enabled the characterization of the conveyor-belt motion of $GABA_A$ receptors in the GC membrane. In the GC central region, $GABA_AR$s randomly alternate between a Brownian movement and a directed motion. Given the values of the diffusion coefficient, $D \approx 0.25\ \mu m^2\ s^{-1}$, and the velocity $v \approx 0.75\ \mu m\ s^{-1}$, during the phases of directed movement, as well as their typical duration, $T \approx 4$ s, these phases cannot be easily detected by eye. Indeed, during T, the distance covered by diffusion $\sqrt{4DT}$ is close to vT, the displacement due to transport.

Other methods have been proposed to detect deviation from a Brownian diffusion in the lateral dynamics of single molecules (11–13). In particular, Saxton theoretically discussed how two parameters, the extent and the anisotropy of the trajectory, could be analyzed to distinguish a directed movement from a random walk, but not in the context of transient effects (17). In fact, the computation of the correlations in speed, combined with the temporal filtering procedure, directly takes into account these two aspects (extent and anisotropy) of the motion in one single parameter.

Pharmacological treatments indicated that the $GABA_AR$ directed movements were microtubule-dependent. The interaction between receptors and MTs possibly occurred at the MT tips and the receptors' motion resulted from the MT dynamics (Fig. 6). This possibility is of particular interest

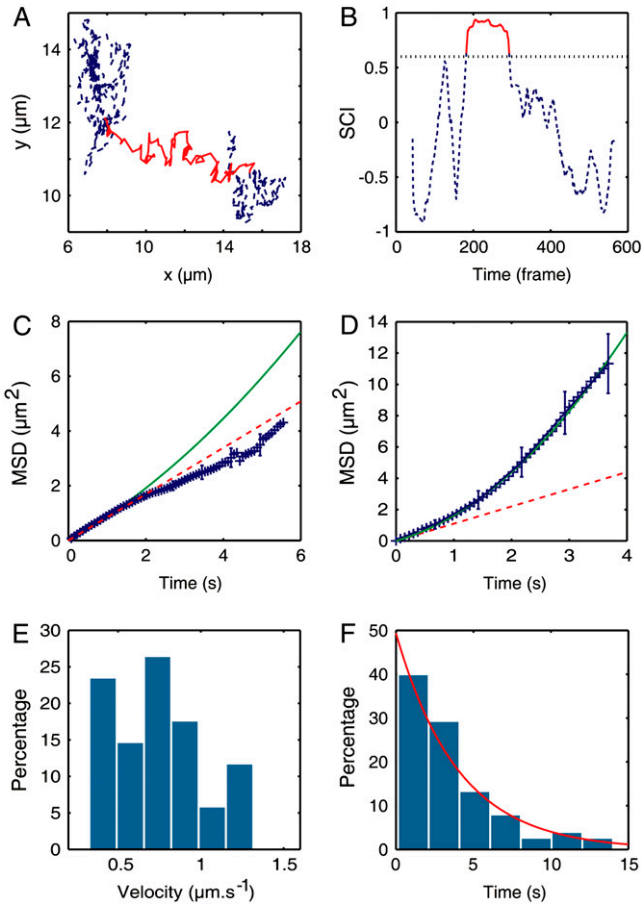

FIGURE 5 (*A*) Example of an experimental trajectory. (*B*) Corresponding SCI. In both graphs, the detected period of directed motion is indicated by the red continuous line. (*C*) Average MSD during the periods identified by the SCI as Brownian with a linear fit $4Dt$, $D = 0.21\ \mu m^2\ s^{-1}$ (*dashed line*). (*D*) Average MSD during the periods identified as directed with a quadratic fit $4Dt + v^2t^2$, $D = 0.26\ \mu m^2\ s^{-1}$ and $v = 0.76\ \mu m^2\ s^{-1}$ (*solid line*). (*E*) Distribution of velocity in the directed periods. (*D*) Distribution of the duration of directed periods adjusted with an exponential curve $\exp(-t/\tau)$ with $\tau = 4.0$ s.

considering the role of proteins binding at MT plus-ends in the regulation of MT stabilization and growth during nerve chemotaxis (26,27). Since no direct coupling between $GABA_A$Rs and MTs has been reported, this interaction is probably mediated by other proteins. Although further experiments are needed to properly identify them, some molecules can already be considered as possible candidates. GABARAP (GABA receptor associated protein) has been shown by immunoprecipitation studies to interact with the $\gamma 2$ subunit of $GABA_A$R and with tubulin (28). It is also involved in the trafficking of receptors to the plasma membrane (29,30). Another possibility is gephyrin, a scaffolding protein (31) involved in the dynamics of $GABA_A$Rs in postsynaptic membranes (32) and known to interact with microtubules.

Our data raise the question of the functional implications of the conveyor-belt motion of $GABA_A$Rs in the membrane. In GCs, activation of $GABA_A$Rs by an external GABA gradient triggers a signaling cascade (33), which leads to growth-

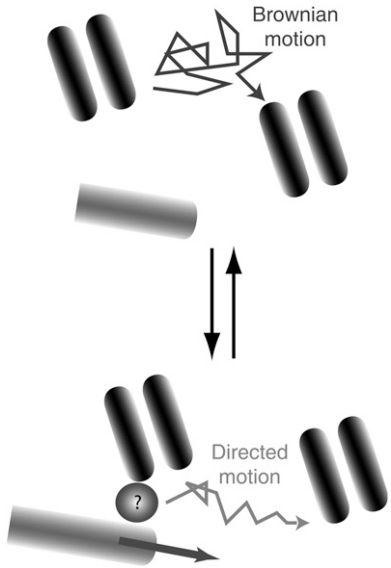

FIGURE 6 Conveyor-belt motion of $GABA_A$Rs in the GC membrane. Receptors switch between free diffusion and MT-dependent directed movement. As a result of this dynamic equilibrium, individual $GABA_A$Rs are displaced with an average velocity of $\sim 0.3\ \mu m\ s^{-1}$. The molecular intermediate (*circle with a question mark*) between receptors and microtubules is not known.

cone steering and elongation (14,15). The coupling between MTs and $GABA_A$Rs suggests that the cytoskeleton is not only a target of the signaling pathway but might also play a role in the regulation of the spatial organization of the signaling molecules and complexes. In other words, receptors could be actively displaced during remodeling of the cytoskeleton, which was induced by their own activation. Compared to trafficking by Brownian diffusion alone, directed transport presents several advantages because it more easily allows the formation of anisotropy in the concentration of molecules and is also a faster process when molecules need to be translocated over large distances.

In the context of GABA gradient sensing, the existence of a feedback loop between the activity of $GABA_A$Rs and their lateral dynamics—mediated by MTs—is an appealing hypothesis. It is supported by the results of experiments showing that, in the presence of a chemoattractant GABA gradient, $GABA_A$Rs redistribute by a MT-dependent mechanism across the GC membrane toward the gradient source (C. Bouzigues, A. Triller, and M. Dahan, unpublished data). The significance of this observation for the sensitivity of gradient sensing by GCs will be discussed in later publications. More generally, the direct coupling between the sensing apparatus and cytoskeletal elements could have a role not only in the detection of nerve chemotaxis but also in biological processes such as synaptic plasticity (35) or the establishment of neuronal polarity (36), where the activity of receptors influence their cytoskeleton-dependent reorganization.

In conclusion, the SCI is a sensitive and quantitative tool, having the potential to be used in a large variety of systems

where transient directed motions are involved, but difficult to extract from the Brownian fluctuations. Combined with advanced single-molecule techniques, it should prove useful for analyzing the trafficking of biomolecules, either in the membrane or in the cytoplasm, and relate their spatial dynamics to functional properties of the cells.

We thank Stéphane Bonneau for his work on trajectory reconstruction and Antoine Triller and Sabine Lévi for their help and fruitful discussions. We are grateful to Marie-Virginie Ehrensperger for her critical reading of the manuscript.

This work was supported by the Centre National de Recherche Scientifique and the Ecole Normale Supérieure.

REFERENCES

1. Dietrich, C., B. Yang, T. Fujiwara, A. Kusumi, and K. Jacobson. 2002. Relationship of lipid rafts to transient confinement zones detected by single particle tracking. *Biophys. J.* 82:274–284.
2. Simson, R., B. Yang, S. E. Moore, P. Doherty, F. S. Walsh, and K. A. Jacobson. 1998. Structural mosaicism on the submicron scale in the plasma membrane. *Biophys. J.* 74:297–308.
3. Lommerse, P. H., G. A. Blab, L. Cognet, G. S. Harms, B. E. Snaar-Jagalska, H. P. Spaink, and T. Schmidt. 2004. Single-molecule imaging of the H-ras membrane-anchor reveals domains in the cytoplasmic leaflet of the cell membrane. *Biophys. J.* 86:609–616.
4. Daumas, F., N. Destainville, C. Millot, A. Lopez, D. Dean, and L. Salome. 2003. Confined diffusion without fences of a G-protein-coupled receptor as revealed by single particle tracking. *Biophys. J.* 84:356–366.
5. Ueda, M., Y. Sako, T. Tanaka, P. Devreotes, and T. Yanagida. 2001. Single-molecule analysis of chemotactic signaling in *Dictyostelium* cells. *Science.* 294:864–867.
6. Dahan, M., S. Lévi, C. Luccardini, P. Rostaing, B. Riveau, and A. Triller. 2003. Diffusion dynamics of glycine receptors revealed by single quantum dot tracking. *Science.* 302:442–445.
7. Tardin, C., L. Cognet, C. Bats, B. Lounis, and D. Choquet. 2003. Direct imaging of lateral movements of AMPA receptors inside synapses. *EMBO J.* 22:4656–4665.
8. Meier, J., C. Vannier, A. Serge, A. Triller, and D. Choquet. 2001. Fast and reversible trapping of surface glycine receptors by gephyrin. *Nat. Neurosci.* 4:253–260.
9. Michalet, X., F. F. Pinaud, L. A. Bentolila, J. M. Tsay, S. Doose, J. J. Li, G. Sundaresan, A. M. Wu, S. S. Gambhir, and S. Weiss. 2005. Quantum dots for live cells, in vivo imaging, and diagnostics. *Science.* 307:538–544.
10. Qian, H., M. P. Sheetz, and E. L. Elson. 1991. Single particle tracking: analysis of diffusion and flow in two-dimensional systems. *Biophys. J.* 60:910–921.
11. Saxton, M. J., and K. Jacobson. 1997. Single-particle tracking: applications to membrane dynamics. *Annu. Rev. Biophys. Biomol. Struct.* 26: 373–399.
12. Simson, R., E. D. Sheets, and K. Jacobson. 1995. Detection of temporary lateral confinement of membrane proteins using single-particle tracking analysis. *Biophys. J.* 69:989–993.
13. Meilhac, N., L. Le Guyader, L. Salome, and N. Destainville. 2006. Detection of confinement and jumps in single-molecule membrane trajectories. *Phys. Rev. E.* 73:011915.
14. Ferguson, S. C., and S. McFarlane. 2002. GABA and development of the *Xenopus* optic projection. *J. Neurobiol.* 51:272–284.
15. Xiang, Y., Y. Li, Z. Zhang, K. Cui, S. Wang, X. B. Yuan, C. P. Wu, M. M. Poo, and S. Duan. 2002. Nerve growth cone guidance mediated by G protein-coupled receptors. *Nat. Neurosci.* 5:843–848.
16. Bray, D. 1998. Signaling complexes: biophysical constraints on intracellular communication. *Annu. Rev. Biophys. Biomol. Struct.* 27:59–75.
17. Saxton, M. J. 1994. Single-particle tracking: models of directed transport. *Biophys. J.* 67:2110–2119.
18. Levi, S., C. Vannier, and A. Triller. 1998. Strychnine-sensitive stabilization of postsynaptic glycine receptor clusters. *J. Cell Sci.* 111:335–345.
19. Bonneau, S., M. Dahan, and L. Cohen. 2005. Single quantum dot tracking based on perceptual grouping using minimal paths in a spatiotemporal volume. *IEEE Trans. Image Process.* 14:1384–1395.
20. Kusumi, A., Y. Sako, and M. Yamamoto. 1993. Confined lateral diffusion of membrane receptors as studied by single particle tracking (nanovid microscopy). Effects of calcium-induced differentiation in cultured epithelial cells. *Biophys. J.* 65:2021–2040.
21. Edidin, M., M. C. Zuniga, and M. P. Sheetz. 1994. Truncation mutants define and locate cytoplasmic barriers to lateral mobility of membrane glycoproteins. *Proc. Natl. Acad. Sci. USA.* 91:3378–3382.
22. Stepanova, T., J. Slemmer, C. C. Hoogenraad, G. Lansbergen, B. Dortland, C. I. De Zeeuw, F. Grosveld, G. van Cappellen, A. Akhmanova, and N. Galjart. 2003. Visualization of microtubule growth in cultured neurons via the use of EB3-GFP (end-binding protein 3-green fluorescent protein). *J. Neurosci.* 23:2655–2664.
23. Lin, C. H., and P. Forscher. 1993. Cytoskeletal remodeling during growth cone-target interactions. *J. Cell Biol.* 121:1369–1383.
24. Salmon, W. C., M. C. Adams, and C. M. Waterman-Storer. 2002. Dual-wavelength fluorescent speckle microscopy reveals coupling of microtubule and actin movements in migrating cells. *J. Cell Biol.* 158:31–37.
25. Zhou, F. Q., C. M. Waterman-Storer, and C. S. Cohan. 2005. Focal loss of actin bundles causes microtubule redistribution and growth cone turning. *J. Cell Biol.* 157:839–849.
26. Kalil K., and E.W. Dent. Touch and go: guidance cues signal to the growth cone cytoskeleton. *Curr. Opin. Neurobiol.* 15:521–526 .
27. Zhou, F. Q., J. Zhou, S. Dedhar, Y. H. Wu, and W. D. Snider. 2004. NGF-induced axon growth is mediated by localized inactivation of GSK-3β and functions of the microtubule plus end binding protein APC. *Neuron.* 42:897–912.
28. Wang, H., F. K. Bedford, N. J. Brandon, S. J. Moss, and R. W. Olsen. 1999. GABA(A)-receptor-associated protein links GABA(A) receptors and the cytoskeleton. *Nature.* 397:69–72.
29. Kittler, J. T., P. Rostaing, G. Schiavo, J. M. Fritschy, R. Olsen, A. Triller, and S. J. Moss. 2001. The subcellular distribution of GABARAP and its ability to interact with NSF suggest a role for this protein in the intracellular transport of GABA(A) receptors. *Mol. Cell. Neurosci.* 18:13–25.
30. Leil, T. A., Z. W. Chen, C. S. Chang, and R. W. Olsen. 2004. GABAA receptor-associated protein traffics GABAA receptors to the plasma membrane in neurons. *J. Neurosci.* 24:11429–11438.
31. Craig, A. M., G. Banker, W. Chang, M. E. McGrath, and A. S. Serpinskaya. 1996. Clustering of gephyrin at GABAergic but not glutamatergic synapses in cultured rat hippocampal neurons. *J. Neurosci.* 16:3166–3177.
32. Jacob, T. C., Y. D. Bogdanov, C. Magnus, R. S. Saliba, J. T. Kittler, P. G. Haydon, and S. J. Moss. 2005. Gephyrin regulates the cell surface dynamics of synaptic GABAA receptors. *J. Neurosci.* 25:10469–10478.
33. Fukura, H., Y. Komiya, and M. Igarashi. 1996. Signaling pathway downstream of GABAA receptor in the growth cone. *J. Neurochem.* 67:1426–1434.
34. Reference deleted in proof.
35. Kneussel, M. 2005. Postsynaptic scaffold proteins at non-synaptic sites. The role of postsynaptic scaffold proteins in motor-protein-receptor complexes. *EMBO Rep.* 6:22–27.
36. Nakada, C., K. Ritchie, Y. Oba, M. Nakamura, Y. Hotta, R. Iino, R. S. Kasai, K. Yamaguchi, T. Fujiwara, and A. Kusumi. 2003. Accumulation of anchored proteins forms membrane diffusion barriers during neuronal polarization. *Nat. Cell Biol.* 5:626–632.